

Computation Method of Gear Dynamic Response Using Experimental Strain Data and Application in Pitting Fault Analysis

Yongzhi Qu¹, Haoliang Zhang², Zechao Wang³, Zude Zhou⁴

^{1,2,3,4}*School of Mechanical and Electronic Engineering, Wuhan University of Technology, Wuhan, Hubei, China, 430070*

¹*Department of Mechanical and Industrial Engineering, University of Minnesota Duluth, Duluth, MN 55812*

*yongzhi@d.umn.edu
1366833634@qq.com*

ABSTRACT

In this paper, A semi-physical method for calculating time varying mesh stiffness and the dynamic response of gear system based on experimental strain data is studied. In a previous work, it was reported that dynamic strain on gear tooth root can be measured under normal operating condition using fiber Bragg Grating (FBG) sensors. This paper aims to compute gear dynamic response using experimental strain data and give an explanation of the fault propagation process. Using the dynamic strain data from FBG sensors, a method for calculating the dynamic response of gear system is proposed. Based on the theory of potential energy and material mechanics, the relationship between the bending strain of the tooth root and the time varying mesh stiffness is established. The time varying mesh stiffness and dynamic response of healthy gear and pitted gear are then calculated respectively. The force transmission during gear mesh under the condition of surface pitting is analyzed. It is concluded that in the case of pitting fault, there will be a significant loss of torque in the power transmission process due to the loss of contact area. It is further inferred that the loss of meshing force and the decreasing of Hertzian contact stiffness are the major contributing factors for pitting fault. In addition, the semi-analytical method of computing gear dynamic response is validated with experimental study of acceleration signal in the perspective of dynamic response.

1. INTRODUCTION

Establishing accurate dynamic model of gear system can help understand fault symptoms and fault generation mechanisms. Tooth surface wear is a common failure mode for gears. When wear fault occurs on the gear tooth, such as pitting and spalling, the dynamic response of gear will be affected.

Therefore, the gear dynamic model with pitting faults has been studied by many researches. Chaari, Baccar, & Abbes (2008) studied the influence of rectangular pitting fault on gear meshing stiffness by assuming rectangular pitting shape on single tooth, and analyzed vibration response spectrum variety by the dynamic response of a 8-degree-of-freedom gear model. The vibration signatures of each tooth fault were then identified. Cheng, Gu, and Qin (2011) devised a gear pitting damage level estimation methodology by integrating a physical model for simulation signal generation, a three-step statistic algorithm for feature selection and damage level estimation for grey relational analysis. The influence of rectangular pitting faults on the vibration response of planetary gear system was investigated and the degree of gear pitting failure was identified. Qu, Zhang, Hong, Tan, and Zhou (2018) evaluated the contribution of mesh stiffness reduction and change of friction on gear dynamic response introduced by surface pitting faults by a 6-degrees-of-freedom spur gear model incorporating the sliding friction and the time-varying mesh stiffness, especially for incipient pitting. The influence of surface pitting on the dynamic response of geared system under light surface pitting was studied analytically and experimentally, the simulation results indicated that the impact of slide friction is significant during the initial pitting stage, However, for sever pitting, the reduction in mesh stiffness is more critical.

Gear mesh stiffness, as one of the major inherent properties of gear system, will directly determine the dynamic response of gear system. Time-varying mesh stiffness is usually calculated by the potential energy. An experimental method for measuring the meshing stiffness of spur gear system based on strain gauge was presented by Raghuwanshi and Parey (2016). The mesh stiffnesses of healthy and cracked spur gear tooth were calculated based on strain energy and strain energy release rate respectively. Then, the meshing stiffness obtained by the experimental method is compared with the meshing stiffness obtained by the energy method, which validated the correctness of the calculation through the experimental method. Pandya and Parey (2013) applied the

FirstAuthorFirstName FirstAuthorLastName et al. This is an open-access article distributed under the terms of the Creative Commons Attribution 3.0 United States License, which permits unrestricted use, distribution, and reproduction in any medium, provided the original author and source are credited.

traditional photoelasticity technique to experimentally measure the meshing stiffness of a pair of spur gears with crack, and the comparisons are made with the finite element method based on linear elastic fracture mechanics. Raghuwanshi and Parey (2015) measured the stress intensity factor of a cracked gear tooth by applying the photoelasticity technique. Then, the stress intensity factor is used to evaluate the gear mesh stiffness. As has been shown in the works (Raghuwanshi & Parey, Pandya & Parey), experimental methods were used to measure the time-varying meshing stiffness of gears, however, all the experiments were only performed under static condition (Liang, Zuo, and Feng, 2018).

In this paper, A semi-physical method for calculating time varying mesh stiffness and the dynamic response of gear system based on experimental strain data is proposed. It aims to compute gear dynamic response using experimental strain data and give an explanation of the fault propagation process. The rest of the paper is organized as follows: Section 2 presents the mesh stiffness calculation method and the gear dynamic model. Section 3 illustrates the gear strain measurement experiments. Section 4 gives the results and discussion. Section 5 concludes the paper.

2. METHOD AND MODELING

2.1 Theory of Gear Meshing Stiffness

Time-varying mesh stiffness, caused by the change of contact tooth number and contact position, is one of the main sources of vibration for gear transmission systems (Liang, Zuo, and Pandey, 2014). For a spur gear pair with contact ratio $\sigma \in (1,2)$, the gear meshing period includes single tooth contact zone (STCZ) and double tooth contact zone (DTCZ). According to (Raghuwanshi & Parey, 2016), the mesh stiffness of single tooth contact zone can be written as:

$$k_m = \frac{1}{\frac{1}{k_p} + \frac{1}{k_h} + \frac{1}{k_g}} \quad (1)$$

where k_p is the pinion tooth stiffness, k_g is the gear tooth stiffness and k_h is the Hertzian contact stiffness. Hertzian contact stiffness can be calculated by Eq. (2) (Liang *et al.* 2016):

$$k_h = \frac{EB\pi}{4(1 - \nu^2)} \quad (2)$$

where E is modulus of elasticity, B is tooth width and ν is Poisson's ratio.

The mesh stiffness of double tooth contact zone can be written as (Raghuwanshi & Parey, 2016):

$$k_m = \frac{1}{\frac{1}{k_{p1}} + \frac{1}{k_h} + \frac{1}{k_{g1}}} + \frac{1}{\frac{1}{k_{p2}} + \frac{1}{k_h} + \frac{1}{k_{g2}}} \quad (3)$$

where k_{p1} is the tooth stiffness of pinion for the first pair of teeth, k_{g1} is the tooth stiffness of gear for the first pair of teeth, k_{p2} is the tooth stiffness of pinion for the second pair of teeth, k_{g2} is the tooth stiffness of gear for the second pair of teeth.

If a tooth in meshing has pitting fault, the stiffness of healthy tooth k_g can be replaced by the stiffness of gear pitting tooth $k_{g_pitting}$. In order to calculate the meshing stiffness of the gear system, each individual tooth stiffness is needed to be evaluated, which can be calculated from experimentally measured gear root strain. Based on (Raghuwanshi & Parey, 2016), a similar gear meshing stiffness calculation method using dynamic strain measurements on gear tooth root is introduced in the next section.

2.2 meshing stiffness calculation method

Base on material mechanics rule: For an elastic body under external force, the energy stored in the elastic body due to the elastic deformation is called elastic strain energy. The elastic strain energy U stored in the volume of the structure can be computed as (Raghuwanshi & Parey, 2016):

$$U = \int_{vol} \frac{\sigma^2}{2E} dV \quad (4)$$

where E is the modulus of elasticity and σ is the stress distribution in the beam.

As the bending stress varies along the height of tooth and depth of tooth, the bending stress σ can be replaced by an average bending stress σ_{av} . And the average bending stress σ_{av} is constant for a given position of load on the tooth profile according to (Raghuwanshi & Parey, 2016). Therefore, the Eq. (4) of the elastic strain energy U can be modified as Eq. (5).

$$U = \int_{vol} \frac{\sigma_{av}^2}{E} dV \quad (5)$$

In gear mechanics analysis, gear teeth are usually considered as a cantilever beam with variable cross section. The bending stress distribution at different cross section along the tooth height can be calculated by Eq. (6).

$$\sigma = \frac{Mc}{I} \quad (6)$$

where M is the bending moment, c is the half tooth thickness of different cross-section and I is the area moment of inertia.

The distribution of bending stress along tooth height by Eq. (6) is shown in Fig. 1, the amplitude of normal force F on the tooth profile is takes as 2.46×10^3 N. The average factor K_{av} can be calculated by the distribution of bending stress and it is constant for a particular load position. K_{av} is defined as the ratio of tooth root stress (σ_{max}) to the average stress along tooth length (σ_{avtl}). σ_{max} is the maximum bending stress occurring at the tooth root and σ_{avtl} is the ratio of the

summation of maximum bending stress at different cross sections along tooth height to the number of cross-section along tooth height (Raghuwanshi & Parey, 2016).

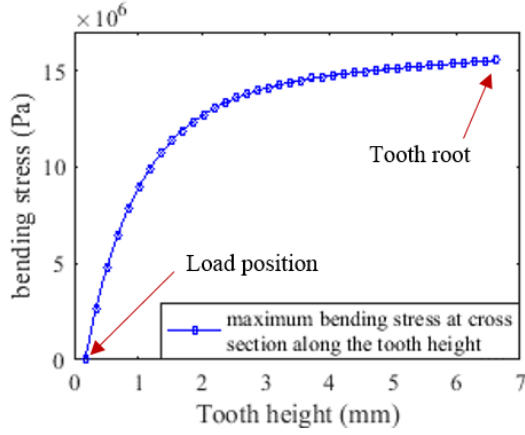


Figure 1. Maximum bending stress at different cross section along tooth height

According to the theory of material mechanics, the bending stress varies linearly along the cross section from neutral axis to top or bottom edge of the cross section of tooth, so the average stress within top or bottom portion of the tooth cross section from the neutral axis will be the half of the maximum stress at the top or bottom edge of the rectangular cross section. the total average bending stress σ_{av} along the tooth height can be written as Eq. (7) by the maximum bending stress σ_{max} at the tooth root (Raghuwanshi & Parey, 2016).

$$\sigma_{av} = \frac{\sigma_{max}}{2K_{av}} \quad (7)$$

Substitute σ_{av} in Eq. (5) by Eq. (7) to build the relationship between the bending stress and the strain energy:

$$U = \int_{vol} \frac{\sigma_{max}^2}{4K_{av}^2 E} dV \quad (8)$$

According to the Hooke's law $\sigma = E\varepsilon$, the Eq. (8) can be written as:

$$U = \int_{vol} \frac{\varepsilon_{max}^2 E}{4K_{av}^2} dV \quad (9)$$

where ε_{max} is the maximum strain at the gear tooth root. Eq. (9) establishes the relationship between the root bending strain and the tooth elastic strain energy. Therefore, the elastic strain energy stored in the gear tooth can be obtained by the tooth root bending strain measured by the strain sensor in the experiment.

According to the potential energy method theory, the stiffness k of gear tooth can be calculated as (Liang, Zhang, Liu and Zuo, 2016):

$$k_{p,g} = \frac{F^2}{2U} \quad (10)$$

where F is the normal force on the gear tooth profile. Eq. (1)-Eq. (10) establishes the relationship between the root bending

strain and the gear meshing stiffness. Therefore, the gear meshing stiffness of can be obtained by the tooth root bending strain measured in the experiment.

The meshing stiffness calculation method of healthy gear based on dynamic strain of tooth root can be written as Eq. (1)-Eq. (10).

When the tooth surface is pitted, the meshing contact line will be corrupted due to the pitting. Since the meshing contact line is intermittent and discontinuous, at the position where pitting occurs, the pinion tooth and gear tooth will no longer transmit full force at those locations, which will result in a loss of torque. When the pitting fault occurs on the tooth surface, the Eq. (6) can be modified as follows:

$$\sigma = \frac{\alpha M c}{I} \quad (11)$$

where α is the loss factor of torque we introduced. α can be expressed as the ratio of the length of actual meshing contact line to tooth width.

Another major change in the presence of pitting is the change in Hertzian contact stiffness. According to (Liang *et al.* 2016), the Hertzian contact stiffness for gear pairs with circular tooth pits can be expressed as:

$$k_h = \frac{\pi E (L - \sum_1^N \Delta L_x)}{4(1 - \nu^2)} \quad (12)$$

where ΔL_x is the reduction of tooth contact width, N is the number of circular pits on a tooth surface.

2.3 dynamic model

To further evaluate the effect of pitting, the dynamic response of the gear system is analyzed. The dynamic model reported in (He, Gunda, & Singh, 2007) is used in this study for gear pitting effect analysis. This model has been used to evaluate dynamic response of the spur gear incorporating the sliding friction and the gear mesh stiffness. It is a mass-spring-damper model with 6 degrees-of-freedom, including rotational motions (θ_p and θ_g), line-of-action translations (x_p and x_g) and off-line-of-action translations (y_p and y_g). The 6 degree-of-freedom model is given below:

$$J_p \ddot{\theta}_p(t) = T_p + \sum_{i=0}^{n=floor(\sigma)} X_{pi}(t) F_{pfi}(t) - \sum_{i=0}^{n=floor(\sigma)} r_{bp} N_{pi}(t) \quad (13)$$

$$J_g \ddot{\theta}_g(t) = -T_g + \sum_{i=0}^{n=floor(\sigma)} X_{gi}(t) F_{gfi}(t) + \sum_{i=0}^{n=floor(\sigma)} r_{bg} N_{gi}(t) \quad (14)$$

$$m_p \ddot{x}_p(t) + 2\xi_{pBx} \sqrt{K_{pBx} m_p} \dot{x}_p(t) + K_{pBx} x_p(t) + \sum_{i=0}^{n=floor(\sigma)} N_{pi}(t) = 0 \quad (15)$$

$$m_g \ddot{x}_g(t) + 2\xi_{gBx} \sqrt{K_{gBx} m_g} \dot{x}_g(t) + K_{gBx} x_g(t) + \sum_{i=0}^{n=floor(\sigma)} N_{gi}(t) = 0 \quad (16)$$

$$m_p \ddot{y}_p(t) + 2\xi_{pBy} \sqrt{K_{pBy} m_p} \dot{y}_p(t) + K_{pBy} y_p(t) - \sum_{i=0}^{n=floor(\sigma)} F_{pfi}(t) = 0 \quad (17)$$

$$m_g \ddot{y}_g(t) + 2\xi_{gBy} \sqrt{K_{gBy} m_g} \dot{y}_g(t) + K_{gBy} y_g(t) - \sum_{i=0}^{n=floor(\sigma)} F_{gfi}(t) = 0 \quad (18)$$

The related notations are listed below:

J_p and J_g denote the polar moment of inertia of the pinion (driving gear) and the gear (driven gear), respectively;
 T_p and T_g denote the torque of the pinion and the gear;
 m_p and m_g denote the mass of the pinion and the gear;
 r_{bp} and r_{bg} denote the radius of base circle of the pinion and the gear;
 θ_p and θ_g denote the rotational angular of the pinion and the gear;
 x_p and x_g denote the displacement along the line-of-action direction of the pinion and the gear;
 y_p and y_g denote the displacement along the off-line-of-action direction of the pinion and the gear;
 K_{pBx} and K_{gBx} denote the effective shaft-bearing stiffness in the line-of-action direction;
 K_{pBy} and K_{gBy} denote the effective shaft-bearing stiffness in the off-line-of-action direction;
 ξ_{pBx} ξ_{pBy} ξ_{gBx} and ξ_{gBy} denote the shaft-bearing damping ratios;
 $X_{pi}(t)$ and $X_{gi}(t)$ denote the moment arm on the pinion and the gear for the friction force;
 $N_{pi}(t)$ and $N_{gi}(t)$ denote the normal forces acting on the pinion and the gear;
 $F_{pfi}(t)$ and $F_{gfi}(t)$ denote the friction forces on the pinion and the gear, $F_{pfi}(t) = \mu N_{pi}(t)$ and $F_{gfi}(t) = \mu N_{gi}(t)$;
 i denotes the gear system acting on the i th meshing tooth pair.

3. THE GEAR STRAIN MEASUREMENT EXPERIMENTS

3.1 Test rig

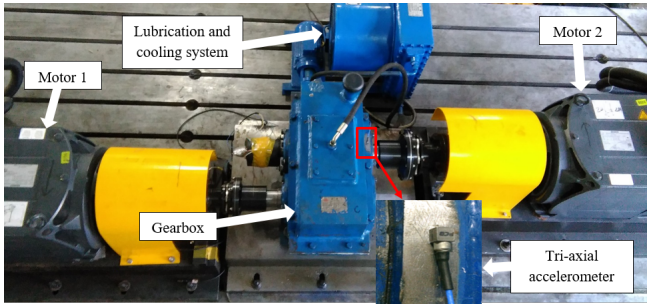


Figure 2. Experiment test rig for gearbox dynamic mesh stiffness analysis

The gear strain measurement experiments were performed on an industrial standard gearbox installed in an electronically closed transmission test rig. The gearbox test rig includes two 45 kW Siemens servo motors. One of the motors can act as the driving motor while the other can be configured as the load motor acting as a generator. The overall test rig is showed in Fig.2. The configuration of the driving mode is flexible. Compared with traditional open loop test rig, the electrically closed test rig is economically more efficient, and can virtually be configured with arbitrary load and speed specifications within rated power. The testing gearbox is a

one stage gearbox with spur gears. The gearbox has a speed reduction rate of 1.8:1. The input driving gear has 40 teeth and the driven gear has 72 teeth. The gear parameters are list in Table 1.

Table 1. List of parameters for gear under testing

Gear parameter	Driving gear	Driven gear
Tooth number	40	72
Module	3 mm	3 mm
Base circle diameter	112.763 mm	202.974 mm
Pitch diameter	120 mm	216 mm
Pressure angle	20°	20°
Addendum coefficient	1	1
Diametral pitch	8.4667	8.4667
Engaged angle	19.7828°	19.7828°
Circular pitch	9.42478 mm	9.42478 mm
Addendum	4.5 mm	3.588 mm
Dedendum	2.25 mm	3.162 mm
Addendum modification factor	0.5	0.196
Addendum modification	1.5 mm	0.588 mm
Fillet radius	0.9 mm	0.9 mm
Tooth thickness	5.8043 mm	5.1404 mm
Tooth width	85 mm	85 mm
Actual center distance	170.002 mm	170.002 mm

3.2 Sensor deployment specifics

In the experiment, two types of sensors were used to monitor the gear system: the vibration sensor for acceleration and the Fiber Bragg Grating (FBG) sensors. Specifically, a tri-axial accelerometer was attached on the gearbox case close to bearing house on the output end to monitor the vibration under different operating conditions of gear, which is also shown in Fig. 2. The sampling rate of the vibration acceleration sensor was 20.48KHz.

All the strain measurements were made on the output driven gear. FBG sensors with a grating length of 5 mm at an interval of 58 mm along the optic fiber were customized to measure distributed gear strains. A total of nine FBG sensors were bonded to the tooth root of gear end face along the base circle for dynamic strain measurements. The details of the sensor deployments are shown in Fig. 3. FBGs were bonded along gear tooth roots using epoxy based adhesive as suggested by the manufacturer. the FBG signals were collected through rotary joints and the FBG signals were sampled at 5 kHz sampling rate.

3.3 Testing condition

Two different gear condition of gear systems are included in the gear strain measurement experiments: healthy gear and pitted gear. The pitting faults were simulated by using electrical discharge machine to erode gear tooth face. The pitting is created on one of the teeth of the output driven gear

after the healthy condition experiment with the same gear. Approximately, the gear tooth face was erode with a depth of 0.5 mm and the radius of 1.5 mm. There are 19 pitting dots of the same degree uniformly distributed along tooth width. The simulated pitting faults are shown in Fig. 4.

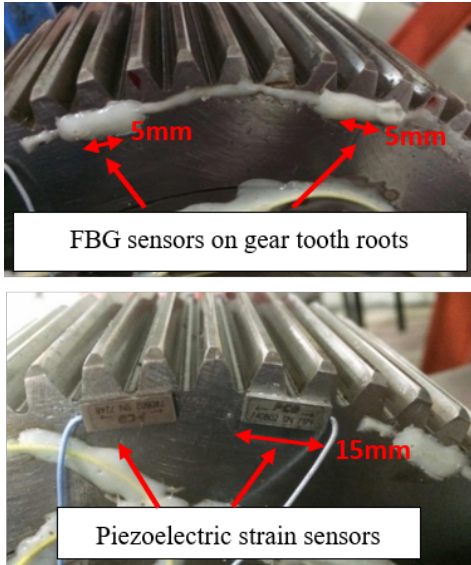


Figure 3. Strain sensor deployment

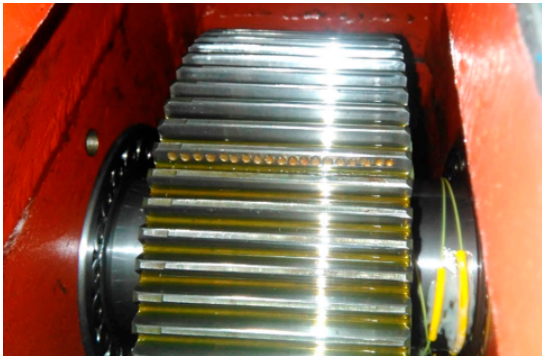


Figure 4. simulated gear pitting fault

With regards to operation conditions, the gearbox was run with the minimum torque of 50 Nm and a maximum of 500 Nm. The minimum speed of the input shaft is 100 rpm and the maximum is 3600 rpm. For each test condition, five samples were collected.

4. RESULTS AND DISCUSSION

The results were shown in the following perspectives: (1) Meshing stiffness calculation based on dynamic strain of tooth root. (2) Dynamic response evaluation using dynamic models. (3) Experimental results analysis.

4.1 Meshing stiffness calculation based on dynamic strain of tooth root

The comparison of strain of the pitted tooth and the healthy tooth measured in the experiments by the FBG sensors is shown in Fig. 5, with the operating condition of input speed 500 rpm and output torque 500 Nm. The detailed experimental results has been reported in (Qu, Hong, Jiang, He, He, Tan, and Zhou, 2017). It can be clearly seen that the tooth pitting caused a loss of strain from the middle part of double tooth contact all the way through single tooth contact zone (Curve BD), which means the pitted tooth is providing less torque. Also, the following compressive stress also see a light decrease (Curve DE). The dynamic strain measurement also indicate that the time varying mesh stiffness will reduce when tooth pitting is presented. The experimental results supported the previous work from (Liang *et al.*, 2016) that pitting will lead to mesh stiffness loss especially in single tooth contact zone.

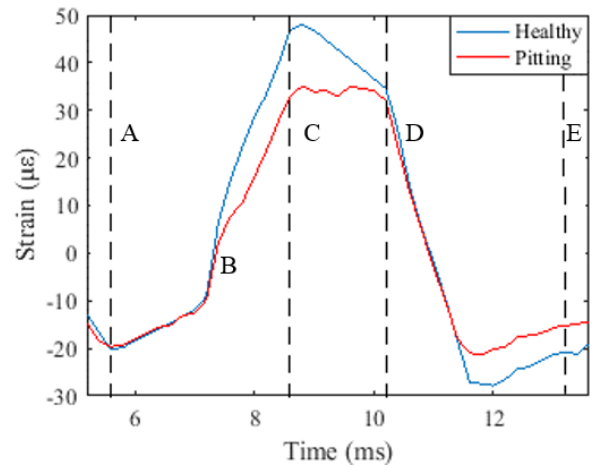


Figure 5. Strain Comparison of Healthy tooth and Pitted tooth

In Section 2.1, the relationship between the root bending strain and the gear meshing stiffness is established. Therefore, the meshing stiffness of the gear can be calculated by the experimentally measured root bending strain.

For a single tooth, the dynamic stress on the dangerous cross section during gear meshing for both healthy gear and pitted gear can be calculated by Eq. (6) and (11), respectively, which are shown in Fig. 6. It can be seen that the tooth pitting will lead to the reduction of the bending stress, the area where the bending stress is significantly reduced is from the middle of double tooth contact all the way through single tooth contact zone. This is consistent with the area where the bending strain of the tooth root decreases (Curve BD) in the experiment. The above analysis shows that the tooth pitting fault will provide smaller torque for gear meshing, and also confirms the rationality of Eq. (11).

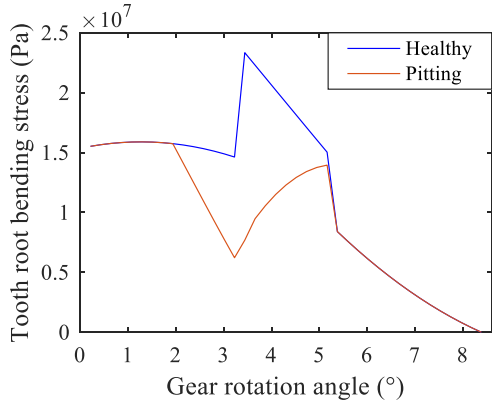


Figure 6. Dynamic stress transition process during the gear meshing

According to Eq. (1-12), the meshing stiffness of the healthy gear and the pitting gear can be calculated by the experimentally measured root bending strain. The results are shown in Fig. 7. The reduction of meshing stiffness of gears is mainly presented in the middle part of the meshing area of double teeth to the end of the meshing area of single teeth and the second meshing area of double teeth. This indicates that the gear pitting will result in reduction of meshing stiffness of gears.

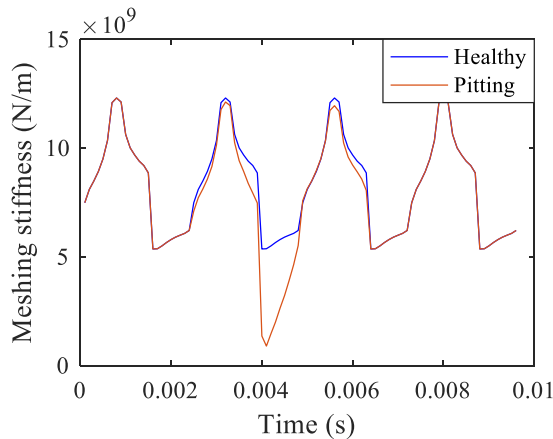


Figure 7. Mesh stiffness for healthy gear and pitting gear

4.2 Dynamic Response Evaluation using Dynamic Models

The TVMS obtained from experimental data is then used as input to a simulation model based on the dynamic model in session 2.3. In the evaluation process, the rotation speed of the pinion is set as 500 rpm and the torque of the gear braking on the output side is set as 500 Nm. The dynamic response results are obtained using MATLAB ode45 function with a sampling frequency of 40000.

In this section, we first compare the result of healthy gear with pitted gear to examine the effect of pitting. Then, some statistical indicators for healthy gear and pitted gear will also be compared.

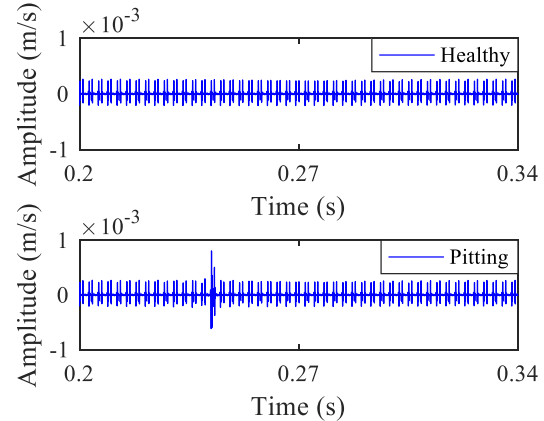


Figure 8. Velocity signals for healthy gear and pitting gear
The simulated velocity signals of the gear system for healthy gears and pitting faulty gears are shown in Fig. 8, the time of signals given in this figure is 0.14s. It can be observed that the response signal of the healthy gear is relatively stable overall in the time domain. However, for the response signal of the pitting faulty gear, the amplitude of the signal increases abnormally in the time domain, which reveals the influence of pitting fault on the dynamic response of gear system.

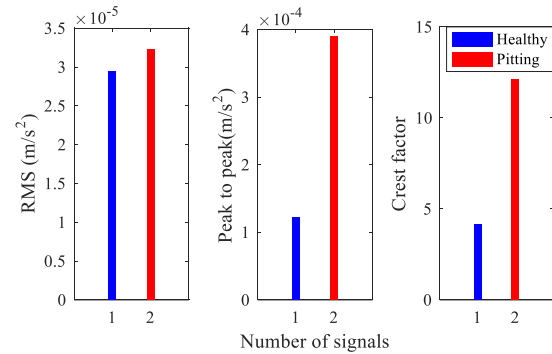


Figure 9. Condition indicators of velocity signals for healthy gear and pitting gears

In order to quantify the statistical characteristics of healthy gear and pitting fault gear response signals, some statistical indicators of dynamic response signals are shown in Fig. 9. The value of RMS, peak-to-peak and crest factor were shown in the bar graph. It can be seen that the dynamic response of the faulty gear has an obviously increased peak-to-peak value and crest factor value.

4.3 Experimental results Analysis

The experimental vibration acceleration signal of the gear system for healthy gears and pitting faulty gears are shown in Fig. 10. It can be seen that the vibration acceleration signal for healthy gear is relatively stable overall in the time domain, and the amplitude is low. However, the vibration acceleration signal of pitting fault gear has a significant increase in amplitude than healthy gear. Abnormal peaks can be obviously observed in the time domain. The above analysis verifies the validity of the simulation model from the time

domain, moreover reveals the influence of the pitting fault on the gearbox system.

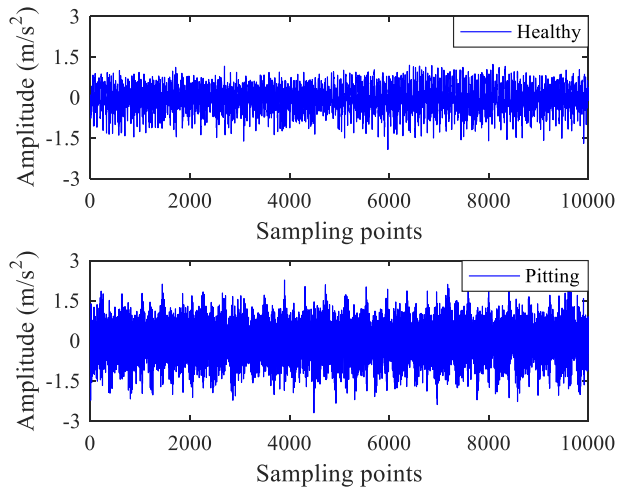


Figure 10. Vibration acceleration signals for healthy gear and pitting gear

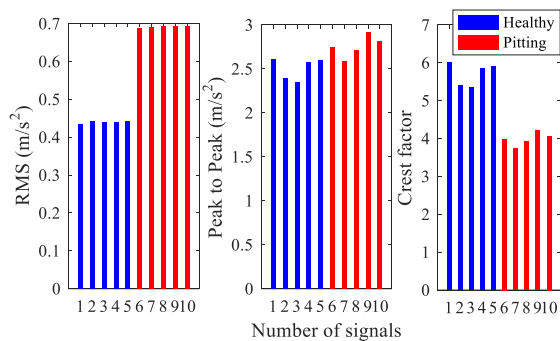


Figure 11. Condition indicators of vibration acceleration signals for healthy gear and pitting gears

The statistical indicators of vibration signals of healthy gears and pitted gears are shown in Fig. 11. It can be seen from the bar graph that the value of RMS and peak-to-peak of the vibration acceleration signal of pitting fault gear are increased compared with healthy gear, which is consistent with the RMS and the peak-to-peak performance of the simulated signal, the difference of RMS value can be more obviously distinguish the gear condition. However, the crest factor of the pitting fault gear is smaller than that of the healthy gear, which is likely caused by external noise during the experiment. It is also interesting to see that the RMS is more effective in analyzing the experimental vibration signals than that in computational results.

5 CONCLUSION

In this paper, a method for calculating the dynamic response of gear system using the dynamic strain data from FBG sensors, was proposed. Based on the theory of potential energy and material mechanics, the relationship between the bending strain of the tooth root and the time varying mesh stiffness was established. The time varying mesh stiffness

and dynamic response of healthy gear and pitted gear were then calculated respectively. It was confirmed that in the case of pitting fault, there would be a significant loss of torque in the power transmission process due to the loss of contact area. It was further inferred that the loss of meshing force and the decreasing of Hertzian contact stiffness were the major contributing factors for pitting fault. In addition, experimental study on acceleration signals also helped to support the semi-analytical method for gear dynamic response computation.

ACKNOWLEDGEMENT

This work was partially supported by the national natural science foundation of China, under project No. 51505353.

REFERENCE

- Chaari, F., Baccar, W., & Abbes, M. S. (2008). Effect of spalling or tooth breakage on gear mesh stiffness and dynamic response of a one-stage spur gear transmission. *European Journal of Mechanics*, 27(4):691-705. doi: 10.1016/j.euromechsol.2007.11.005
- Cheng, Z., Hu, N., Gu, F., & Qin, G. (2011). Pitting damage levels estimation for planetary gear sets based on model simulation and grey relational analysis. *Transactions-Canadian Society for Mechanical Engineering*, 35(3):403-417. doi:10.1139/tcsme-2011-0023
- Qu, Y., Zhang, H., Hong, L., Tan, Y., & Zhou, Z. (2018). Dynamic Modeling and Fault Feature Analysis of Pitted Gear System. 2018 IEEE International Conference on Prognostics and Health Management (ICPHM). doi:10.1109/icphm.2018.8448451
- Raghuwanshi, N. K., & Parey, A. (2016). Experimental measurement of gear mesh stiffness of cracked spur gear by strain gauge technique. *Measurement*, 86, 266–275. doi:10.1016/j.measurement.2016.03.001
- Pandya, Y., & Parey, A. (2013). Experimental investigation of spur gear tooth mesh stiffness in the presence of crack using photoelasticity technique. *Engineering Failure Analysis*, 34, 488-500. doi: 10.1016/j.engfailanal.2013.07.005
- Raghuwanshi, N. K., & Parey, A. (2015). Mesh stiffness measurement of cracked spur gear by photoelasticity technique. *Measurement*, 73, 439-452. doi:10.1016/j.measurement.2015.05.0
- Liang, X., Zuo, M. J., & Feng, Z. (2018). Dynamic modeling of gearbox faults: A review. *Mechanical Systems and Signal Processing*, 98, 852–876. doi:10.1016/j.ymsp.2017.05.024
- Liang, X., Zuo, M. J., & Pandey, M. (2014). Analytically evaluating the influence of crack on the mesh stiffness of a planetary gear set. *Mechanism and Machine Theory*, 76, 20–38. doi:10.1016/j.mechmachtheory.2014.02.001

- Liang, X., Zhang, H., Liu, L., & Zuo, M. J. (2016). The influence of tooth pitting on the mesh stiffness of a pair of external spur gears. *Mechanism and Machine Theory*, 106, 1–15. doi:10.1016/j.mechmachtheory.2016.08.005
- He, S., Gunda, R., & Singh, R. (2007). Effect of sliding friction on the dynamics of spur gear pair with realistic time-varying stiffness. *Journal of Sound and Vibration*, 301(3-5), 927–949. doi:10.1016/j.jsv.2006.10.043
- Liang, X., Zhang, H., Liu, L., & Zuo, M. J. (2016). The influence of tooth pitting on the mesh stiffness of a pair of external spur gears. *Mechanism and Machine Theory*, 106, 1–15. doi:10.1016/j.mechmachtheory.2016.08.005
- Qu, Y., Hong, L., Jiang, X., He, M., He, D., Tan, Y., & Zhou, Z. (2017). Experimental study of dynamic strain for gear tooth using fiber Bragg gratings and piezoelectric strain sensors. *Proceedings of the Institution of Mechanical Engineers, Part C: Journal of Mechanical Engineering Science*, 095440621774400. doi:10.1177/0954406217744000